Quantitative thermography: a powerful but simple tool to assess the fatigue strength of metals in a one-specimen test–capabilities and limitations in the test setup

Received 23 May 2022
Revised 17 September 2022
Accepted 10 October 2022

Jonas Rauber, Christian Motz and Florian Schaefer
Department of Materials Science and Methods, Saarland University, Saarbrücken, Germany

Abstract

Purpose – The aim of the study is the question, that is, which evaluation method for the measured temperature profile is more suitable and feasible for quantitative thermometry (QT): A simple measurement setup based on 3-point temperature sensing by means of semiconductor sensors (NTCs) or thermographic methods which offer 2-dimensional (2D) temperature measurements of the sample with good spatial resolution but an inferior temperature sensitivity. What experimental effort is required to adjust the test setup to satisfy the boundary conditions of the underlying thermodynamic equations?

Design/methodology/approach – In this paper results of both methods are contrasted and the error of QT measurement is assessed by finite element analysis (FEA) in this follow-up.

Findings – The low-cost NTC method allows a straightforward determination of a lower estimate of the fatigue strength with only a very small measurement error. Even asymmetries in the thermal boundary conditions of the test setup are broadly tolerated, as well as a lack of thermal isolation.

Practical implications – The method is restricted to metallic materials without phase transitions during fatigue in the fatigue strength regime.

Originality/value – QT is not a new method. The assessment of the methods proposed in the literature regarding their practicability in terms of accuracy is innovative focus of this work. Nevertheless, highly accurate thermometric measurements can be performed by using simple commercial sensors in combination with a standard digital multimeter.

Keywords Mechanical behavior of materials, Strength of materials, Fatigue, Thermometry

Paper type Research paper

1. Context and motivation

Fatigue of metallic materials is still one of the major challenges in material design, especially regarding sustainable component and part engineering. With decreasing applied load amplitudes, one approaches the regime of fatigue strength of materials, where life-time is determined by the crack initiation phase (Goto, 1992).

In the high cycle fatigue (HCF) range the determined material fatigue strength is subject to large scatter. Therefore, a large amount of specimens, at least 10, should be tested for proper determination of fatigue strength (Hück, 1983; Müller *et al.*, 2014), making testing time intensive. Reducing excessive testing times by increasing the load frequency always runs the risk of introducing artifacts, since most materials are strain rate sensitive. Increasing the load frequency also leads to increased heat dissipation and the specimen temperature

The authors thank Dr. Michael Roland from Applied Mechanics at Saarland University for the fruitful discussion about fitting tools in MATLAB. The authors thank Dres.-Ing. Peter Starke and Hoaron Wu from Hochschule Kaiserslautern for their support during data acquisition with the IR camera.

Funding: No funding was received.

Competing interests: There are no competing interests.

International Journal of Structural Integrity

1757-9864
DOI 10.1108/IJSI-05-2022-0074

cannot be considered as constant. This can cause large errors in the determined fatigue strength. Therefore, a fast and more cost-effective method is desired to estimate the fatigue strength.

The deformation processes in the fatigue strength regime that eventually lead to damage, i.e. to crack initiation, dissipate energy and thus impact the heat generation within the specimen (Staerk, 1980, 1982a; Schaefer *et al.*, 2022a). Quantitative thermometry (QT) uses this effect that is detrimental for conventional fatigue testing, to its advantage: The dissipation generated by damage is used to assess internal deformation states within the specimen (Starke *et al.*, 2006, 2010).

The thermometric approach to evaluate material damage has been developed since fatigue research became more and more important at the beginning of the last century (Stromeyer, 1914; Dengel and Harig, 1980). Initially, as sensor sensitivity and electronic processing improved, the resolution of the QT increased. Thus, heat generation below the onset of plasticity due to anelastic effects could already be measured (Mareau *et al.*, 2012). Fundamental work on semiconductor temperature sensors with negative temperature coefficient (NTC) in combination with a load-increase test (LIT) was provided by Staerk (1980) and Staerk (1982a, b). However, Staerk's work was only published in German.

As infrared (IR) camera technology became more available, it has been increasingly used to asses fatigue damage due to their ability to provide 2-dimensional (2D) data, despite their lower thermal sensitivity (Luong, 1998; Guo *et al.*, 2015; Teng *et al.*, 2020; Jung *et al.*, 2019). At the same time, thermocouples were also employed. Their comparatively low sensitivity required the use of temperature-controlled specimen clamping to achieve constant and symmetrical thermal boundary conditions (Starke *et al.*, 2006, 2010). As long as such boundary conditions are met, the curvature of the recorded temperature profile along the specimen surface is directly linked to the amount of heat generation within the specimen as shown by the early thermometric studies from Staerk (1980). The temperature itself, however, is not sufficient to characterize fatigue damage (Meneghetti, 2007), although the temperature in the middle of a standard uniaxial specimen represents obviously the curvature of the evolving temperature profile and hence the heat generation within the specimen in the case of symmetrical temperature boundary conditions, i.e. a symmetrical temperature of the fixtures. Indeed, this is hard to achieve perfectly.

In recent years, there has been an increased focus on the analysis of thermographic data (Luong, 1998; Jung *et al.*, 2018). The low thermal resolution of IR cameras allows detecting local damage sites but prohibits unlocalized damage assessment below the fatigue strength regime. Unfortunately, this has contributed to the common misconception that heat generation below the fatigue strength regime is negligible (La Rosa and Risitano, 2000).

Thus far, the sensitivity of NTCs is unsurpassed. Yet, both methods, the NTC-QT and the IR-QT, are fundamentally different in their requirements and limitations for a testing setup. Using NTCs, a specimen can be thermally isolated, which is practically not possible for using an IR camera.

Hence, 3 questions arise:

(1) Does the test results really benefit from a more elaborated test setup such as clamping thermostats or excessive thermal isolation as mentioned and used by many authors?

(2) How stable is the evaluation with both methods under asymmetric thermal boundary conditions due to the experimental setup?

(3) Is a simple parabolic fit, were 3 sample points of the temperature profile suffice, as proposed by Staerk (1982a) as suitable as a more complex double-exponential fit derived from a one-dimensional heat equation that needs more or less continuous

temperature profile data (Guo *et al.*, 2015; Schaefer *et al.*, 2022a) regarding the two questions above?

First, a concise overview of the fundamental thermodynamic equations and their simplifications for practicable application is given, followed by an explanation of the NTC-QT methodology in comparison to the IR-QT methodology using a short recap of our previous work on the topic, already published in more detail by Schaefer *et al.* (2022a, b). The effects of application errors in the NTCs as well as deviations from the theoretical assumptions about the thermal boundary conditions are investigated using finite element analysis (FEA) regarding the already published experimental results.

2. Thermodynamic background

The mechanical hysteresis in fatigue of metallic materials reflects the dissipation of energy inside the material, most of which is dissipated as thermal energy. This continuous heat flux causes the temperature within the specimen to rise.

Assuming a constant mass density $\rho = \rho(\mathbf{r}, t)$ and a constant heat capacity $C = C(\mathbf{r}, t)$, the temperature $T = T(\mathbf{r}, t)$ at the position $\mathbf{r}$ at time t is given by Boulanger *et al.* (2004).

$$\rho C\dot{T} - \nabla(k(\mathbf{r})\nabla T) = d_1(\mathbf{r}, t) + s_{the}(\mathbf{r}, t) + s_{ic}(\mathbf{r}, t) + r_{ext}(\mathbf{r}, t) \tag{1}$$

here, k denotes the heat conduction tensor that is assumed to be constant, even for changes in temperature, and isotropic, and therefore $k = k_{ij} = k\delta_{ij}$. This assumption holds especially true for most metallic materials and for heat generation in the fatigue strength regime where an increase in temperature is usually below 1 °C. Furthermore, s_{ic} denotes an internal coupling source that characterizes e.g. contributions from microstructural changes to the heat flux. In the fatigue strength regime, microstructural changes are minimal and contribute only negligibly to heat generation. Therefore, the internal coupling source s_{ic} is assumed to vanish. r_{ext} denotes an external heat supply from the surroundings, such as thermal convection and radiation, and s_{the} the thermoelastic source and d_1 the heat flux from mechanical dissipation. Therefore, Eq. (1) is simplified to

$$\rho C\frac{\partial\theta}{\partial t} - k\Delta\theta = s = s_{the} + d_1 + r_{ext} \tag{2}$$

with the temperature variation $\theta = T - T_0$. W may also assume that the contribution of external heat sources r_{ext} is time-independent and is vanishing according to Boulanger *et al.* (2004) and Teng *et al.* (2020). This could be implemented in the experimental setup e.g. by an appropriate specimen isolation. In the following, we will use finite element (FE) simulation to investigate the extent to which r_{ext}, a contribution from thermal radiation and convection, distorts this assumption.

The actual distribution of heat sources in a 3D specimen is unknown. Assuming that the surface temperature and the average depth-dependent temperature are equal, that means that the averaged heat source is representative for what happens throughout the thickness, Boulanger *et al.* introduced a mean heat source for each cross section. From integration of the heat conduction Eq. (2) to the second and third spatial dimension leads to a 1D diffusion equation. It follows

$$\rho C\left(\frac{\partial\theta}{\partial t} + \frac{\theta}{\tau_{th}}\right) - k\frac{\partial^2\theta}{\partial x_1^2} = s \tag{3}$$

with the approximations

$$\rho C \frac{\theta}{\tau_{th}} \approx -\frac{k}{e}\left[\frac{\partial \theta}{\partial x_i}\right]_{-e/2}^{e/2} \tag{4}$$

for each dimension x_i. This claims uniform and linear Fourier heat conduction conditions especially at the specimen boundaries which means that the heat losses are proportional to the temperature variation θ. τ_{th} then describes the heat losses through the specimen surface by radiation and convection at $x_i = \pm\frac{e}{2}$.

If the fatigue load function is periodic with frequency f, starting the load cycle i at t_i, Eq. (3) can be further averaged.

$$\begin{cases} \bar{d}_1(i) = f\int_{t_i}^{t_i+1/f} d_1(\tau)d\tau & (5) \\ \bar{\theta}(x_1,i) = f\int_{t_i}^{t_i+1/f} \theta(x,\tau)d\tau & (6) \\ \int_{t_i}^{t_i+1/f} s_{the}(\tau)d\tau = 0 & (7) \\ \int_{t_i}^{t_i+1/f} \dfrac{\partial\theta(x_1,\tau)}{\partial\tau}d\tau = 0 & (8) \end{cases}$$

which finally leads to the averaged 1D heat equation for isolated, homogeneous and isotropic specimens

$$\rho C \frac{\overline{\theta}(x_1,i)}{\tau_{th}^{1D}} - k\frac{\partial^2\overline{\theta}(x_1,i)}{\partial x^2} = \overline{d_1}(i) \tag{9}$$

Eq. (9) is a second-order linear differential equation. A solution is

$$\overline{\theta}(x_1,i) = a_1(i)e^{b(i)x_1} + a_2(i)e^{-b(i)x_1} + c(i) \tag{10}$$

with

$$c(i) = \frac{\tau_{th}\overline{d_1}(i)}{\rho C} \text{ and } b(i) = \sqrt{\frac{\rho C}{k\tau^{th}}} \tag{11}$$

So, the heat flux or heat generation (≈dissipation) per load cycle $\tilde{q}$ is

$$\tilde{q} = \overline{d_1}(i) = \frac{kb(i)^2c(i)}{f} \tag{12}$$

hence, $\tilde{q}$ can be deduced from a fit to the temperature profile of load cycle i or at time $t(i)$ in a quasi-steady state e.g. measured by thermography. However, the specimen surface cannot be isolated then in contradiction to the assumption of $r_{ext} = 0$. If heat exchange with the specimen's surroundings by convection and radiation is strictly prohibited by thermal (adiabatic conditions), τ_{th} tends to infinity and Eq. (9) simplifies to

$$\tilde{q}(i) + k\frac{\partial^2\overline{\theta}(x_1, i)}{\partial x_1^2} = 0 \tag{13}$$

with the second-order polynomial solution

$$\overline{\theta}(x_1, i) = -\frac{\dot{q}}{2k}x_1^2 + mx_1 + n \tag{14}$$

that can also be achieved using just 3 distinct measuring points for the temperatures using NTCs as already described by Schaefer *et al.* (2022a).

3. Experimental methods and results

3.1 Measurement of temperature profiles

The methodology and experimental data presented here are taken from Schaefer *et al.* (2022a, b), where they are described in more detail.

Continuous load amplitude increase tests (LITs) were performed on a Rumul Mikrotron resonance testing machine from Russenberger Pruefmaschinen AG at a stress ratio R of -1 and a test frequency of about 200 Hz. All tests were carried out at room temperature of 25 °C and the relative air moisture was measured to be below 30%.

Thermographic images were acquired with a capture rate of 1 Hz using the IR camera thermoIMAGER (TIM) 450 from microepsilon providing a thermal sensitivity of 0.04 K at room temperature with an image resolution of 382×288 pixel^2. The magnification was calculated from the distance between the camera and the uniaxial dogbone-shaped specimen with a parallel length of 10 mm. The specimen surface was coated with graphite to achieve a good emissivity near 1. Before starting the test the emissivity was determined by measuring the temperature of the specimen at two different temperatures with a thermocouple and adjusting the temperature calibration of the IR camera until it reads the same temperature value and difference. The temperature profiles along the specimen's length are obtained by averaging the temperature data points over the width of the specimens.

The miniature NTC thermistor from TE (GAGA10KM3499J15) with a reference resistance of 10 $k\Omega$ at room temperature were each calibrated before the test in a water thermostat bath with well-known reference temperature. The NTC array was attached to the specimen in a layered electrical insulating composite. The electric resistance of the NTCs was measured using a Keithley Digital Multimeter DMM 199 with a resolution of 0.001 Ω (0.1 Ω in a 30 $k\Omega$ range) and readout with LabVIEW® using a GPIB2USB adapter from National Instruments. All data evaluation and calculations were done with MATLAB®.

More experimental results, from different material and other stress ratios than $R = -1$, as well as more details on the test setup can be found in Schaefer *et al.* (2022a).

3.2 Specimen and tests

Load increase testing with simultaneous temperature measurement was performed on two flat dogbone-shaped tensile specimens each with a parallel length of 20 mm: One made of S235JR steel and one made of Nickel with a purity of more than 99.999%. The Nickel specimen was treated at 1,200 °C under vacuum to produce a coarse grain microstructure. Both specimen were ground and polished to 1 micron with SiC grinding and diamond polishing suspensions. Temperature was measured by recording the front face of the specimen with the IR camera and in case of the steel sample also with NTCs attached to its back face. Since the IR camera requires the specimen surface to be free and radiating, the specimens could not be isolated.

3.3 Evaluation of the heat generation during fatigue

For the Nickel specimen $\tilde{q}$ was obtained by fitting a second order polynomial to the temperature profiles $T(x)$ from IR-QT as well as a to the three data points from NTC-QT. The values of $\tilde{q}$ retrieved for both measurement techniques were then compared to one another as displayed in Figure 1a). For steel specimen the heat generation per cycle $\tilde{q}$ was obtained by fitting a double-exponential Eq. (12) as well as a second order polynomial Eq. (14) to the temperature profiles $T(x)$ from IR-QT. The fits were compared to the raw data $T(x)$ as displayed in Figure 2. The values of $\tilde{q}$ retrieved via both fitting approaches were contrasted to one another as displayed in Figure 1b).

3.4 Experimental results

The heat values calculated from the IR-QT of the nickel specimen with both fitting approaches almost perfectly coincide; see Figure 1a). This is surprising since the parabolic formulation according to Eq. (14) assumes that there is no thermal interaction between the specimen and its surrounding via thermal convection and radiation (adiabatic conditions). Due to the lacking isolation of the nickel samples this prerequisite was not met.

The IR-QT lacks the outstanding thermal resolution of the NTC-QT. This results in temperature scattering and a higher base-level of $\tilde{q}$ as values below 1,200 J/m^3 are practically not measurable, see Figure 1b). The knee-point in the curve of $\log(\tilde{q})$ over the stress amplitude marks the onset of plasticity and thus the lower limit of the fatigue strength regime. Due to the lower thermal resolution of the IR-QT it runs the risk of failing to resolve the onset of damage and thus special attention must be paid to thermal sensitivity of the sensors.

All measured temperature profiles and heat generations are in good agreement with the results already published by Schaefer *et al.* (2022b).

4. Finite element analysis

As discussed in section 2 Staerk's parabolic formulation of the temperature distribution (Eq. (14)) is only valid if no heat transfer occurs from the sample surface to the environment, i.e. if the specimen is perfectly isolated Staerk (1980). These adiabatic conditions are not achievable in a real experiment which raises the question to what extend radiation and convection impact the accuracy of the measurement. To asses this impact a FEA model was used to calculate exact temperature profiles for selected boundary conditions and analyze

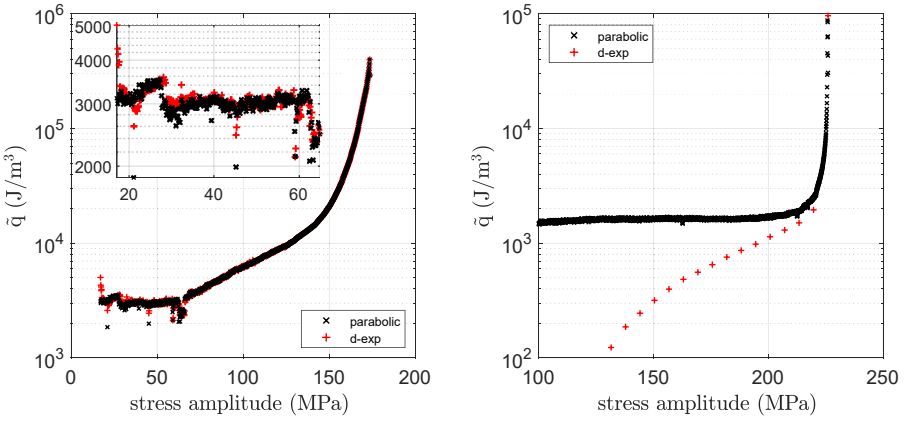

Figure 1.
(a) Comparison of $\tilde{q}$ calculated by parabolic and double-exponential fitting of IR-QT data of the Nickel specimen over the stress amplitude from continuous LIT. Deviations between both curves are very small and just visible by zooming in (inset); (b) Comparison of $\tilde{q}$ from IR-QT data and NTC-QT data of the nickel specimen over the stress amplitude from continuous LIT. For both data sets $\tilde{q}$ was calculated by parabolic fitting. The temperature profiles are gathered by IR-QT on the front of the S235JR steel specimen. The inferior measurement resolution of the IR-QT method is obvious because $\tilde{q}$-values below 1,200 J/m^3 cannot be measured with IR-QT

them with the parabolic (Eq. (14)) as well as the more physically grounded double-exponential formulation (Eqs (10) and (12)), to calculate the magnitude of the internal heat source. In practice, as described throughout section 3, one would use the parabolic formulation for NTC-QT and the double-exponential formulation for IR-QT.

4.1 Model and analysis procedure

All FEA simulations were carried out in Abaqus CAE using a rather simplistic model of a rod shaped steel sample of 50 mm in length and 10 mm in diameter as depicted in Figure 3a). Heat generation due to cyclic plastic deformation was modeled as a constant body heat flux q over the entire volume of the sample assuming a loading frequency of 200 Hz. The ambient temperature T_{amb} was set to 300 K in all cases. Heat transfer over the clamps was modeled by setting the top and bottom surfaces A_L and A_R to a constant temperature. Heat exchange with the environment was modeled for three specific cases:

(1) A perfectly insulated specimen with no interaction at all

(2) A radiating specimen with an emissivity ε_M of 1 (i.e. black body as a worst case scenario) at the mantle face A_M

(3) A radiating sample that also dissipates heat via convection with a film coefficient α_M of 4 W/m^{2}K at the mantle face A_M

When heat exchange with the environment is allowed one must also take into account asymmetries in the temperature profile. In a real setup these may arise due to different rates of heat transfer at the clamps (e.g. because of a strain gauge on one side). This introduces temperature gradient superimposed onto the temperature profile produces by heat generation. In the model this gradient was realized by increasing the temperature at the surface A_R by a temperature offset of ΔT. While the parabolic formulation is in principle capable of accounting for a linear gradient, heat exchange with the environment will cause the gradient to be nonlinear as radiation and convection scale with the temperature difference of the surface to the environment.

Three distinct series of simulations where performed:

(1) no temperature gradient ($\Delta T = 0$ K) over a vast range of heat fluxes.

(2) a constant low heat flux over a range of different ΔT.

(3) a constant high heat flux over a range of different ΔT.

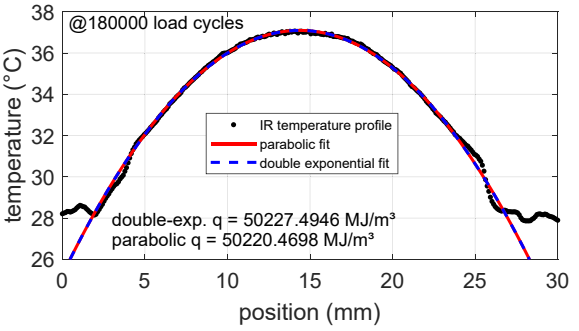

Figure 2. Temperature profile and double-exponential fit for coarse-grained Nickel measured by IR thermography, averaged along the specimen width. The double-exponential fit was done between the positions 8 and 22 mm and is in good agreement with the raw temperature data. The noisy and oscillating temperature at the edges of the data result forms the specimen shoulders and the clamping that show a small temperature difference of the clamps and hence an asymmetry in the thermal boundary conditions

For each simulation the resulting steady state temperatures were extracted along a path x on the sample surface and exported for further analysis in MATLAB. Since the temperature distribution shows the same radial symmetry as the specimen, extraction along a simple straight line is sufficient. From these temperature profiles $T(x)$ the ambient temperature T_{amb} was subtracted and the heat generated per cycle $\tilde{q}$ was calculated for both, the parabolic and double-exponential, formulation. For the former only three points at $x = -25$ mm, $x = 0$ and $x = 25$ mm were used to approximate the usage of just three NTCs. The calculated cyclical heat generation $\tilde{q}_{calc}$ was then compared to the actual value set in the corresponding simulation $\tilde{q}_{real}$ to calculate the relative systematic error $\delta_{sys}\tilde{q}_{calc}$ as

$$\delta_{sys}\tilde{q}_{calc} = \frac{\tilde{q}_{calc} - \tilde{q}_{real}}{\tilde{q}_{real}}$$

4.2 Impact of the heat flux

For series A ($\Delta T = 0$) the simulations were performed for different values of $\tilde{q}_{real}$ ranging from 20 J/m^3 up to 2,000,000 J/m^3 per cycle. These limits were chosen to cover the entire range of values observed in the real specimen in Figure 1a and b. At first glance in Figure 4a) both approaches yield calculated values that almost perfectly coincide with the actual ones in all three cases. For the isolated case 1, this remains true for both fitting approaches, when regarding the relative systematic error as depicted in Figure 4b which remains close to zero for the entire range of $\tilde{q}_{real}$. For the other cases that allow heat exchange with the environment, however, stark differences become apparent. To major regimes can be discerned: Below 20,000 J/m^3 the error remains more or less constant with the double-exponential approach achieving values close to zero and the parabolic approach underestimating $\tilde{q}$ by about 1% for case 2 and 1.6% for case 3. This behavior is to be expected since the heat exchange with the environment flattens the temperature profile and changes is shape away from that of a parabola. Thus the curvature is lower and the parabolic approach yields a $\tilde{q}_{calc}$ hat is lower than $\tilde{q}_{real}$. Above 20,000 J/m^3 the magnitude of the errors begins to greatly increase with increasing $\tilde{q}_{real}$ for both fitting approaches. In both cases this can be attributed to radiation following the Stefan–Boltzmann law according to which the radiant flux $P(x)$ at a given point on our model is given as

$$P(x) = \sigma_B \varepsilon_M \left(T(x)^4 - T_{amb}^4 \right) \tag{15}$$

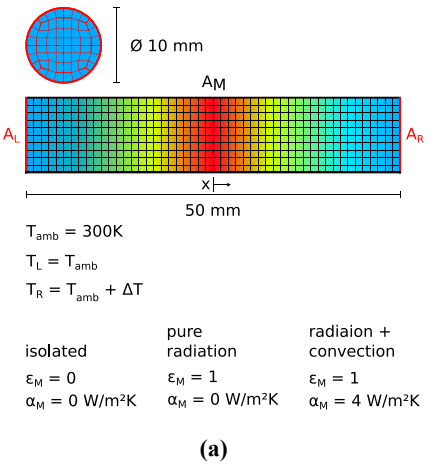

Figure 3.
(a) Schematic of the FEA model. This mesh only serves to display the overall mesh geometry. The actual global mesh size was 0.25 mm, leading to about 400 elements in length, 40 elements in diameter and 124 elements in circumference at the surface. The chosen element type was the DC3D20 quadratic heat transfer brick; (b) Temperature profile for low and high values of heat release per cycle $\tilde{q}$ for low and high temperature offsets ΔT

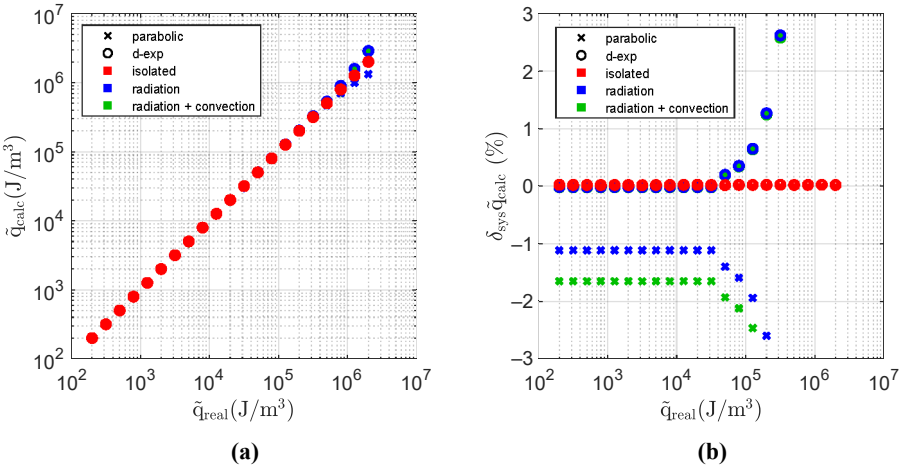

Figure 4.
(a) Calculated heat per cycle over actual heat per cycle for cases 1 to 3 of series A; (b) Systematic error over actual heat per cycle for cases 1 to 3 of series A

with σ_B being the Stefan-Boltzman constant. The parabolic approach continues to underestimate $\tilde{q}_{real}$, but as surface temperatures now exceed 330 K, and the radiant flux scales with $T(x)^4$ radiation begins to dominate the shape of the temperature profile. The double-exponential approach on the other hand, begins to greatly exaggerate $\tilde{q}$. The reasoning for the increasing magnitude of the error of the parabolic approach cannot be directly applied here, since the double-exponential approach should in theory be able to handle environmental heat exchange. However, as discussed in the context of Eq. (3) this heat exchange must also conform to certain boundary conditions–specifically uniform and linear heat conduction. Heat radiation accordingly does violate this condition due to the $T(x)^4$ scaling of the radiation flux.

4.3 Impact of an external temperature gradient

For series B and C the $\tilde{q}_{real}$ was set to a constant value of 200 J/m^3 and 20,000 J/m^3 and the temperature offset ΔT was varied over a range of 0 K up to 5 K. As depicted in Figure 5, the double-exponential approach appears to be perfectly capable to accommodate the introduced

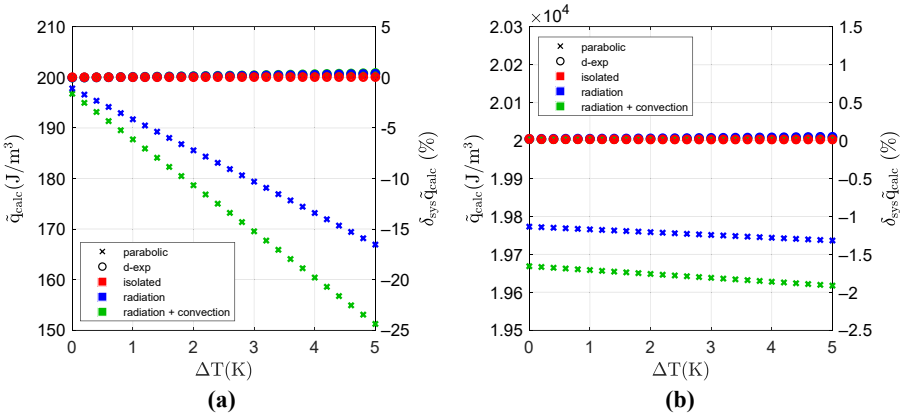

Figure 5.
a) Calculated heat per cycle and systematic error ΔT at $\tilde{q}_{real}$ 200 J/m^3 (series B); (b) Calculated heat per cycle and systematic error ΔT at $\tilde{q}_{real}$ 20,000 J/m^3 series C

temperature gradient regardless of the interaction case and $\tilde{q}_{real}$ and produces relative errors close to 0% in all simulations. The parabolic approach only reaches this level of accuracy for the isolated case A. For the lower $\tilde{q}_{real}$ the relative error sharply increases to up to 16% for case B and 25% for case C. Fort the higher $\tilde{q}_{real}$ the error is much less dependent of ΔT and only changes slightly, staying in a range between 1.0% and 1.25% for case B and 1.5%–1.75% for case C and thus roughly at the level already observed in the previous section. The severe impact of temperature gradients at low heat generation rates may be explained by the fact that the introduced gradient is magnitudes higher than the temperature increase that is caused by the heat source. Therefore the temperature profile is dominated by the gradient as can be seen in Figure 3b). Due to radiation and convection this gradient is nonlinear as already mentioned in section 4.1 and leads to large errors when using the parabolic approach. With increasing $\tilde{q}_{real}$ this error decreases as the external gradient becomes more and more negligible compared to the impact of the heat source.

5. Conclusion

We demonstrated also in previous work that, due to its low thermal resolution, IR-QT may be incapable of determining the onset point of the fatigue strength regime as no knee point may be discernible in the $\tilde{q}$ over stress amplitude profile, see Figure 1b). The use of NTC-QT circumvents this problem as it offers a far superior thermal resolution.

The NTC-QT only measures few points on the specimen surface and thus relies on the parabolic approach to determine $\tilde{q}$. As the parabolic approach assumes perfect isolation from the environment, errors are to be expected as soon as this very strict requirement is not met. Surprisinglyin the experimental tests already published, there was no obvious error, when comparing the $\tilde{q}$ values, that were calculated applying both fitting approaches to the IR temperature data of the nickel samples, that had no thermal isolation whatsoever.

In the present work, the FEA now showed, that even in a worst case scenario, the relative error introduced by using the parabolic approach over the double-exponential one is rather small at values of about 1.6% for low to high values of $\tilde{q}$ as long as no temperature gradient across the sample is introduced. For excessively high values of $\tilde{q}$ both fitting approaches result in large errors, as heat radiation majorly impacts the surface temperature. Temperature gradients as they cannot be avoided in experimental work completely were shown to only marginally impact the relative errors in $\tilde{q}$ if $\tilde{q}$ is large. But they cause massive errors if $\tilde{q}$ is low. I.e. within the range were the usage of NTC-QT over IR-QT may be favorable, a temperature gradient will produce massive errors if the specimen is not isolated.

Therefore, as long as care is taken to properly thermally isolate the specimen, we can still confidently support the use of the easy-to-implement NTC-QT method. This method allows a lower estimate for the fatigue strength for a wide range of metallic materials to be obtained quickly and inexpensively. This is a valuable contribution for parameter studies in the development of sustainable materials. In this context, the high-precision determination of the amount of heat generated gives a precise insight into the deformation processes in a material. In future studies, the complex interaction between deformation mechanisms and damage can thus be investigated in more detail.

References

Boulanger, T., Chrysochoos, A., Mabru, C. and Galtier, A. (2004), "Calorimetric analysis of dissipative and thermoelastic effects associated with the fatigue behavior of steels", *International Journal of Fatigue*, Vol. 26 No. 3, pp. 221-229.

Dengel, D. and Harig, H. (1980), "Estimation of the fatigue limit by progressively-increasing load tests", *Fatigue and Fracture of Engineering Materials and Structures*, Vol. 3 No. 2, pp. 113-128.

Goto, M. (1992), "Scatter characteristics of fatigue life and the behaviour of small cracks", *Fatigue and Fracture of Engineering Materials and Structures*, Vol. 15 No. 10, pp. 953-963.

Guo, Q., Guo, X., Fan, J., Syed, R. and Wu, C. (2015), "An energy method for rapid evaluation of high-cycle fatigue parameters based on intrinsic dissipation", *International Journal of Fatigue*, Vol. 80, pp. 136-144.

Hück, M. (1983), "Ein verbessertes verfahren für die auswertung von treppenstufenversuchen", *Materialwissenschaft und Werkstofftechnik*, Vol. 14 No. 12, pp. 406-417.

Jung, A., Bronder, S., Diebels, S., Schmidt, M. and Seelecke, S. (2018), "Thermographic investigation of strain rate effects in al foams and ni/al hybrid foams", *Materials and Design*, Vol. 160, pp. 363-370.

Jung, A., Al Majthoub, K., Jochum, C., Kirsch, S.-M., Welsch, F., Seelecke, S. and Diebels, S. (2019), "Correlative digital image correlation and infrared thermography measurements for the investigation of the mesoscopic deformation behaviour of foams", *Journal of the Mechanics and Physics of Solids*, Vol. 130, pp. 165-180.

La Rosa, G. and Risitano, A. (2000), "Thermographic methodology for rapid determination of the fatigue limit of materials and mechanical components", *International Journal of Fatigue*, Vol. 22 No. 1, pp. 65-73.

Luong, M.P. (1998), "Fatigue limit evaluation of metals using an infrared thermographic technique", *Mechanics of Materials*, Vol. 28 Nos 1-4, pp. 155-163.

Mareau, C., Favier, V., Weber, B., Galtier, A. and Berveiller, M. (2012), "Micromechanical modeling of the interactions between the microstructure and the dissipative deformation mechanisms in steels under cyclic loading", *International Journal of Plasticity*, Vol. 32, pp. 106-120.

Meneghetti, G. (2007), "Analysis of the fatigue strength of a stainless steel based on the energy dissipation", *International Journal of Fatigue*, Vol. 29 No. 1, pp. 81-94.

Müller, C., Hinkelmann, K., Masendorf, R. and Esderts, A. (2014), "Zur treffsicherheit der experimentellen dauerfestigkeitsschätzung", *TU Clausthal Fakultät*, Vol. 3.

Schaefer, F., Rosar, J., Wu, H., Starke, P. and Marx, M. (2022a), "Obtaining a lower estimate of the fatigue limit of metals by a simplified quantitative thermometric approach in a low-cost one-specimen test", *International Journal of Fatigue*, Vol. 159, pp. 106-729.

Schaefer, F., Rosar, J., Marx, M., Herter, F., Wu, H. and Starke, P. (2022b), "Quantitative thermometry: a revived simplified approach to fatigue strength determination and deformation mechanisms", *Procedia Structural Integrity*, Vol. 37, pp. 299-306.

Staerk, K. (1980), "Thermometrische untersuchungen zum zyklischen verformungsverhalten metallischer werkstoffe", Dissertation Universität Stuttgart, PhD thesis, IWMF, Stuttgart.

Staerk, K.F. (1982a), "Einsatz von heißleiter-temperaturfühlern in der werkstoffprüfung", *Materialwissenschaft und Werkstofftechnik*, Vol. 13 No. 9, pp. 309-313.

Staerk, K.F. (1982b), "Temperaturmessung an schwingend beanspruchten werkstoffen", *Materialwissenschaft und Werkstofftechnik*, Vol. 13 No. 10, pp. 333-338.

Starke, P., Walther, F. and Eifler, D. (2006), "Phybal—a new method for lifetime prediction based on strain, temperature and electrical measurements", *International Journal of Fatigue*, Vol. 28 No. 9, pp. 1028-1036.

Starke, P., Walther, F. and Eifler, D. (2010), "Phybal" a short-time procedure for a reliable fatigue life calculation", *Advanced Engineering Materials*, Vol. 12 No. 4, pp. 276-282.

Stromeyer, C. (1914), "The determination of fatigue limits under alternating stress conditions", *Proceedings of the Royal Society of London. Series A, Containing Papers of a Mathematical and Physical Character*, Vol. 90 No. 620, pp. 411-425.

Teng, Z., Wu, H., Boller, C. and Starke, P. (2020), "Thermography in high cycle fatigue short-term evaluation procedures applied to a medium carbon steel", *Fatigue and Fracture of Engineering Materials and Structures*, Vol. 43 No. 3, pp. 515-526.

Corresponding author
Florian Schaefer can be contacted at: f.schaefer@matsci.uni-sb.de